

Computational Physics Exam

Ludvig Lous

April 2022

1 Introduction

The atomic magnetic moments, or "spins", of particles can be modelled with the Heisenberg model. In the Heisenberg model, the spin can point in all possible directions on the unit sphere. This requires the spin components to be normalized such that they fit on the unit sphere.

The derivative of the spins $\partial_t \mathbf{S}_j$ were calculated using the Landau-Lifschitz-Gilbert (LLG) equation

$$\partial_t \mathbf{S}_j = \frac{-\gamma}{1 + \alpha^2} [\mathbf{S}_j \times \mathbf{F}_j + \alpha \mathbf{S}_j \times (\mathbf{S}_j \times \mathbf{F}_j)] \quad (1)$$

where γ is a gyromagnetic constant, α is the damping constant, \mathbf{S}_j is spin number j and \mathbf{F}_j is the effective field which is described by $\mathbf{F}_j = \mathbf{F}_j^{eff} + \mathbf{F}_j^{th}$ where \mathbf{F}_j^{eff} is described as

$$\mathbf{F}_j^{eff} = -\frac{1}{\mu_s} \frac{\delta H}{\delta \mathbf{S}_j} \quad (2)$$

where H is the Hamiltonian of the system. In other words, \mathbf{F}_j^{eff} is the functional derivative of the Hamiltonian with respect to the spin at site j. By deriving the Hamiltonian, which is described as equation (1) in the exam paper, you get the expression

$$\mathbf{F}_j^{eff} = \frac{1}{\mu_s} \left[\sum_k^N J_{jk} \mathbf{S}_k + 2d_z (\mathbf{S}_j \cdot \hat{\mathbf{e}}_z) \hat{\mathbf{e}}_z + \mu_s \mathbf{B}_j \right] \quad (3)$$

for \mathbf{F}_j^{eff} . J_{jk} is the coupling constant between the spins, \mathbf{S}_k is the neighboring spins, d_z is an anisotropic term, and \mathbf{B}_j is a magnetic field.

\mathbf{F}_j^{th} can be described as

$$\mathbf{F}_j^{th} = \Gamma(t) \sqrt{\frac{2\alpha k_B T}{\gamma \mu_s \Delta t}} \quad (4)$$

The new spin of the particle after a time step was found using the Heun method. The first step of the Heun method is to estimate a new spin value $y_{\tau+1}^p$ using the equation

$$y_{\tau+1}^p = y_\tau + \Delta t f(t_\tau, y_\tau) \quad (5)$$

where y_τ is the current spin value, Δt is the time step and t_τ is the current time. $f(t, y)$ is the LLG equation. The second step of the method estimates the next spin value by taking the average of the LLG equation with the current spin value and the predicted spin values.

$$y_{\tau+1} = y_\tau + \frac{\Delta t}{2} [f(t_\tau, y_\tau) + f(t_{\tau+1}, y_{\tau+1}^p)] \quad (6)$$

Python was used to simulate the spins. The extension Numba, which translates python and numpy code into machine code was also used in order to shorten run time.

2 Single Spin Dynamics

The first task was to simulate the spin of a single particle, thus no nearest neighbour interactions had to be accounted for, and the J term of equation (3) vanishes. The temperature was also set to zero, and thus \mathbf{F}_j^{th} vanishes as well. As the damping factor α was

set to zero, the second term of equation(1) vanishes as well. The simulation of the single particle was done by first implementing a normalization function which normalized any set of spin components by projecting them onto a unit sphere.

The evolution of the three spin components over time is shown in Figure 1. As the damping factor α is zero, the z component of the spin remains constant, while the x- and y-components oscillate around the unit circle.

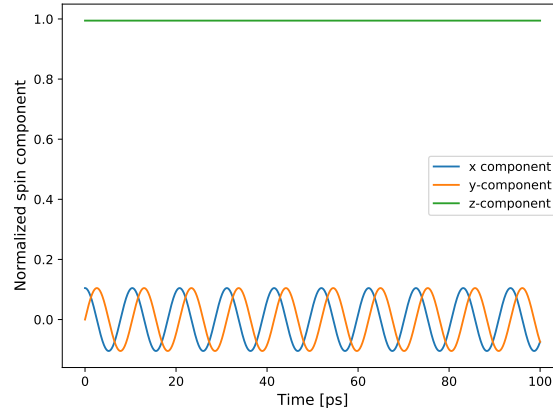


Figure 1: Plots of the x, y and z-components of the spin of a single particle. The z-component stays constant, while the x- and y components oscillate with the same frequency. Their combined length stays constant.

The single particle spin simulation was later conducted in the damped case. Here, the damping factor α was set to 0.1, such that the second term of equation 1 comes into effect. The plots of the x- and y components are shown in Figure 2. Here, one can clearly see that the x- and y components of the spin decay over time towards zero.

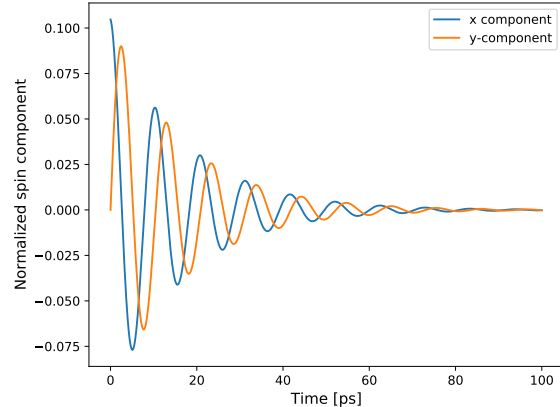


Figure 2: Plot of the x- and y components of the spin of a particle with a damping factor α of 0.1. They oscillate with the same frequency, however they decay towards zero over time.

For ferromagnets, the damping factor is related to the frequency ω and the decay constant τ by the relation

$$\alpha = \frac{1}{\omega\tau} \quad (7)$$

The frequency and the decay constant of the x-component was estimated using the curve_fit function from `scipy.optimize`. This function takes in a function as a parameter and changes the parameters of the function until it fits with the other function. Due to the shape of the oscillation of the x-component, this was predicted to be an equation of the form

$$A \cos(\omega t) e^{-\frac{t}{\tau}} \quad (8)$$

where A is the amplitude of the function. The curve fitted function was estimated to have an A of 0.105, ω of 0.601 and τ of 16.652. From (7) this results in a damping factor α of 0.099. This is in good accordance with the actual damping factor of 0.1. The curve fitted function is plotted together with the x component of the spin in Figure 3. The estimated function seems to fit almost perfectly, which is reflected well in the estimation of α .

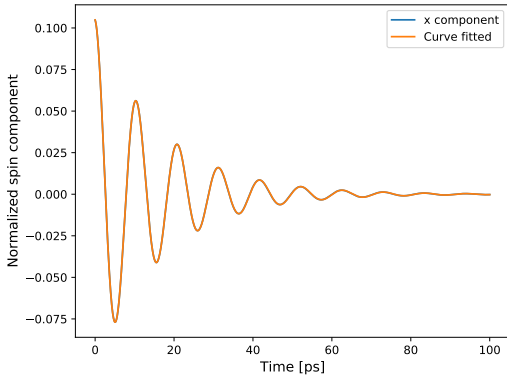


Figure 3: Plot of the x-component of the spin with the curve-fitted function plotted above.

The z-component of the spin is shown in Figure 4, as expected, the z-component increases as the x- and y components decreases. Without any neighbour interactions, the spin of the particle is seen to revert back the z-axis of the unit sphere. One can also see that the derivative of the z-component of the spin decreases as the z-component approaches one. In my simulations of the single particle, the anisotropic term d_z was used. This term will drive the spin component towards the z-direction it is already pointing towards. If I had used the magnetic field component instead, the spin would always revert back to the positive z direction.

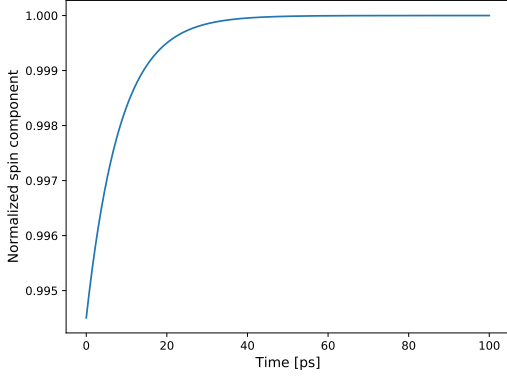


Figure 4: Plot of the z-component of the spin over time. The z-component increases towards 1 over time.

A visualisation of how the spin changes over time for both $\alpha = 0$ and $\alpha > 0$ is given in Figure 5. It should be noted that the initial spin in this figure is different than for the plots above, this figure is mainly intended to give a better visualization of the spin over time. For $\alpha = 0$ the spin turns in a counter-clockwise direction at a constant height, while for $\alpha > 0$ the spin spirals in towards the positive z-pole of the unit sphere.

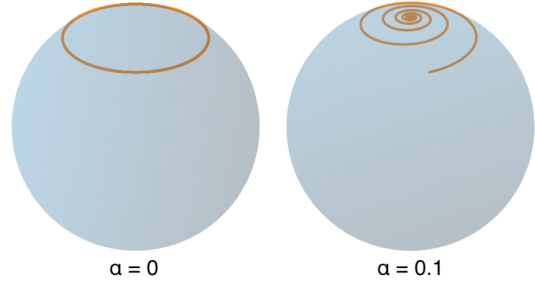


Figure 5: Plot of the total spin over time for no damping factor (left) and a damping factor of 0.1 (right).

3 Linear Chain

The spin simulations was later implemented for a linear chain of spins. In this case, neighbour interactions has to be accounted for, which meant that the J term of equation (3) would be non-zero. The LLG function was modified in order to account for the neighbour interaction term. The Heisenberg coupling J was assumed to be constant between all particles, and was set to 1 meV. In this simulation, only nearest neighbour interactions were accounted for.

I assumed that in the second step of the Heun method (6), the LLG equation with the predicted spin would also take in the predicted spins for the neighbours. Therefore i calculated the predicted spins for all particles in the chain between each time step using (5), and then using these predicted values in (6). In order to make sure the indexing of the neighbours would be correct for both periodic and non-periodic boundary conditions, I made a function which returned the correct neighbouring spins for each spin in the chain. This function had a boolean parameter,

which would return the right neighbours in the case of periodic=True or periodic=False.

A chain consisting of 100 spins in the positive z-direction was created, then the first spin in the chain was excited by tilting the spin slightly away from the z-direction. The change of the x, y and z components of the spins over time are shown in Figure 7. Here, the initial condition is at the bottom of the images, then the spins for each subsequent time step are shown above. Particularly for the z-components, one can see that the excitation of the first spin induces an excitation in the neighbouring spin. However, the wave of excitations fades away before reaching the end of the chain. This is caused by the damping factor α , which was set to 0.01. The spins are not in phase, and the precess back to the z-axis relatively fast.

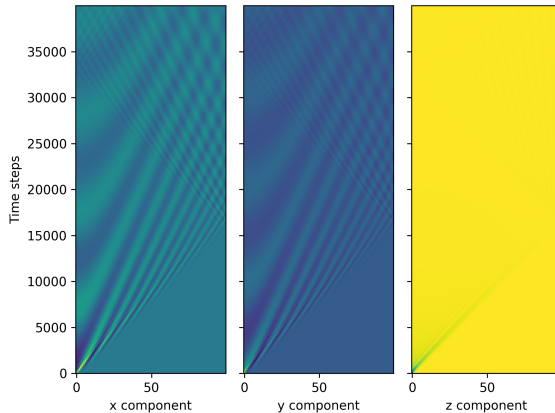


Figure 6: The change in the x, y and z components of the spins are shows over time with a dampening factor of 0.01. The spins were recorded over 40000 time steps, equal to 40 ps.

The same simulation was conducted with the damping factor α set to zero. The results are shown in Figure 7. Here, one can see that the excitation wave in the z-component bounces from end to end of the chain. The wave also seems to disperse over time, which indicates that the spins does not have the same frequency.

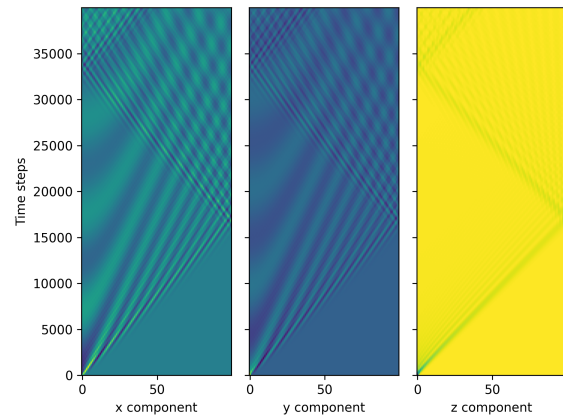


Figure 7: The changes in the x, y and z components of the spins with no dampening factor are shown over 40 ps.

Finally, the simulating was conducted with periodic boundary conditions. The main difference here is that the wave also travels between spin number 1 and N. The excitation wave travels through the chain in periods of around 17 ps, which fits well with the calculated value from the curve_fit results in problem b. Although the damping factor is different, the period seems to stay the same.

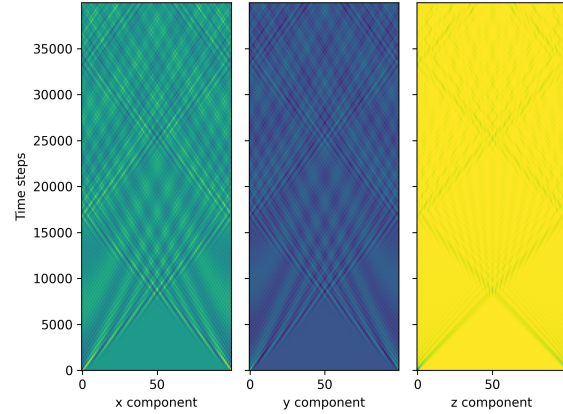


Figure 8: The changes in the x, y and z components of the spin with periodic boundary conditions are plotted over 40 ps.

Another initial spin chain with randomly oriented spins was also created. The random spins were created by creating three uniformly distributed random numbers between -1 and 1 for each spin component, and then normalizing the components. When checking the results, however, the distribution of spins seemed to agglomerate are some regions of the sphere. This is probably due to the uniform distribution taking random coordinates from a unit cell with a volume of 8. Although these numbers are uniformly distributed in the cell, the are not when projected onto the sphere, as points from the corners outside of the sphere gets projected onto the sphere, meaning a larger amount of point are generated at these regions of the sphere. The solution was to reject random numbers which had a vector length of more than one. This ensured that all randomly generated points lied inside the sphere. A comparison of the two distribution is shown in Figure 9. Each sphere has 5000 points on its surface. The chain was then to be simulated over time until it reached equilibrium. This was to be done for both a ferromagnetic chain with a coupling constant $J > 0$ and with an antiferromagnetic chain with a coupling constant $J < 0$. The coupling constant was set to ± 1 meV.

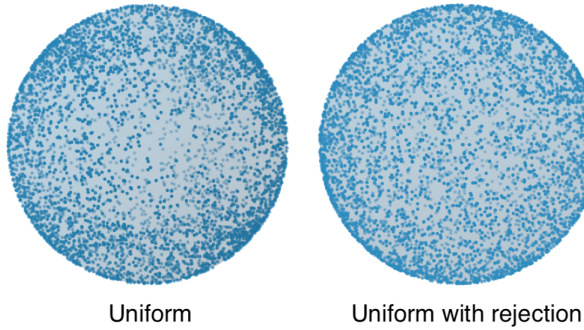


Figure 9: Comparison of random numbers generated on the unit sphere with and without rejection. The unit sphere without rejection has a lower density of points on the region facing the reader, and a higher density at the corners.

The evolution of the spins in the ferromagnetic chain is shown in Figure 10. After around 100 ps,

the spins forms stable phases, where some regions of the chain has spins aligned in the positive z-direction (light green), while other regions has spins oriented in the negative z-direction (dark blue). The theory states that all spins should point in the same direction at equilibrium. In the simulations, however, the are seen to form phases. This could be due to the d_z term being included, and not the B_0 term. As the d_z term favours spins in the directions they are already pointing in, it would seem reasonable that they form such phases. The x- and y components of the spin are also seen to oscillate between having values of 0 and 1 at the left side of the plot with periods of roughly 10 ps.

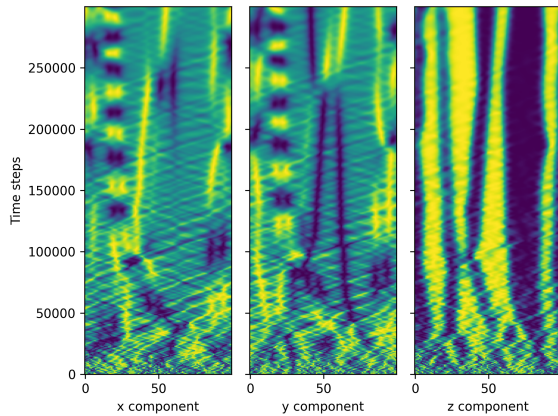


Figure 10: Evolution of a randomly oriented spins in a ferromagnetic chain. The z-components form relatively stable phases after 50-100 ps. The light green areas represents values of 1, while the dark blue areas represents values of -1.

The change in time of the antiferromagnetic chain is shown in Figure 11. After 50 ps, most of the spins have stabilized in alternating directions on the z-axis. These results is in good accordance with the theory, which predicts spins alternating in the positive and the negative z-direction. The x- and y components has values of almost zero at equilibrium, as all z components has a value of either 1 or -1 in the z-axis

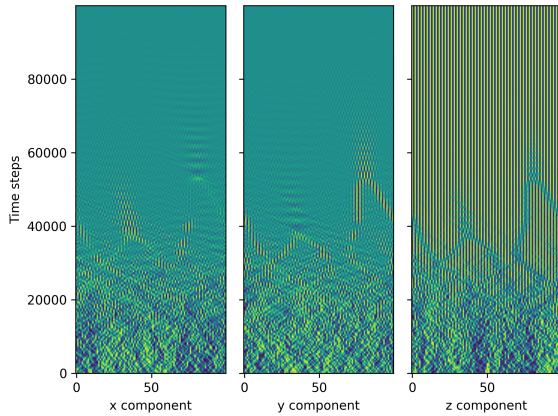


Figure 11: Evolution of a randomly oriented spins in a antiferromagnetic chain. The light green areas has represents values of 1, while the dark blue areas represents values of -1.

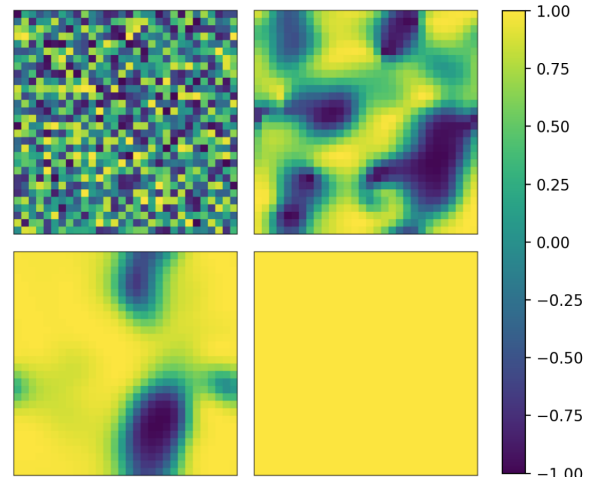


Figure 12: Evolution of the lattice towards equilibrium. The figure shows the initial, randomly oriented spins (top left), the spins after 5 ps (top right), the spins after 10 ps (bottom left) and the spins after 30 ps (bottom right).

4 Two Dimensional Lattice

Next, the spin simulations was implemented for a two dimensional square lattice. A new LLG function which accounted for neighbours below and above in the lattice was created, the term for the magnetic field contribution was also added. A new function to handle the indexing was also created, which handled the right indexing for neighbours of spins at the edges of the lattice. Periodic boundary conditions was assumed in all tasks.

The ferromagnetic ground state was found for the two dimensional lattice as well, by first creating a 30x30 lattice with randomly oriented spins with the same method as in the one-dimensional case. The damping constant α was increased to 0.2. Figure 12 shows how the spins in the lattice changed over time. Contrary to the one-dimensional case, all spins eventually aligned with the positive z-direction. This could be due to the added magnetic field term which only contributes in the positive z-direction, or the doubling of nearest neighbours for all spins.

The time dependent magnetization $M(T, t)$ of a 25x25 lattice with all spins pointing in the positive z-direction was plotted over 30 ps. $k_B T$ was set to be 0.05 J . The results are shown in Figure 13. The temporal average $M(T) = \langle M(T, t) \rangle_t$ of the time dependent magnetization was calculated by taking the average value from 5 to 20 ps, as the magnetization seemed to have stable fluctuations around a constant value after this time. $M(T)$ was estimated to be 0.9910, with a standard deviation of 0.0005.

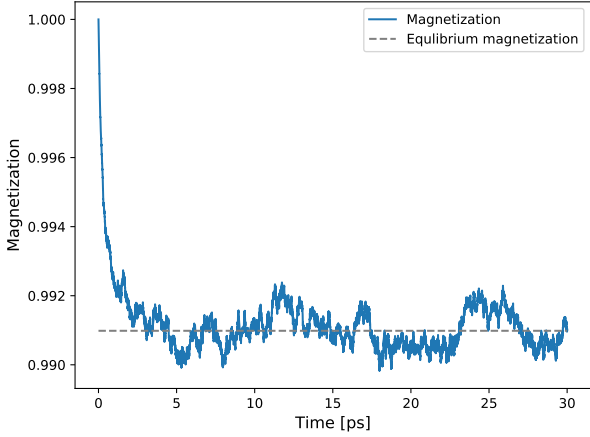


Figure 13: Plot of the time-dependent magnetization of a 25x25 lattice with $k_B T = 0.05 \text{ J}$

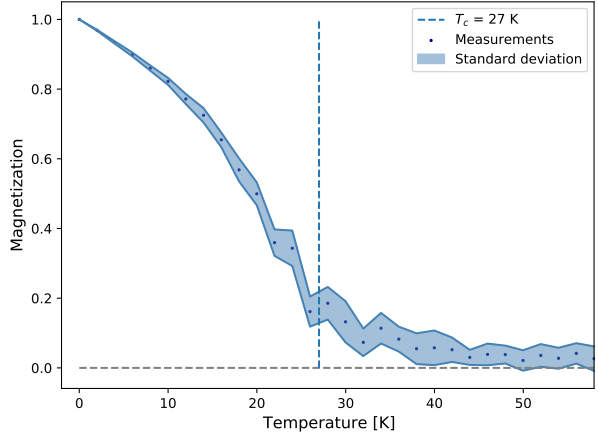


Figure 14: Plot of the temperature dependence of the magnetization at $\mu_s B_0 = 0.1 \text{ J}$. The Curie temperature T_c was estimated to be 27 Kelvin.

The temporal average with respect to T was estimated for 25x25 lattices by finding the temporal average as described above for energies from 0 to $5 k_B T$, which corresponds to temperatures between 0 to 58 Kelvin. J was set as 1 meV, α was set at 0.2, and $\mu_s B_0$ was set as 0.1 meV. The results are shown in Figure 14. A lattice size of 25x25 and 30000 time steps was chosen. This took approximately one hour to simulate. The Curie temperature T_c was estimated to be 27 Kelvin. Above this temperature, the material becomes paramagnetic, while at temperatures below T_c the material is ferromagnetic. T_c was taken at the inflection point of the plot. The standard deviation of the measurements increased with the temperature. This is to be expected, as the thermal noise term increases with the square root of the temperature as seen in Equation (6) in the exam paper.

The magnetization was plotted again in the same way, but this time the magnitude of the magnetic field was increased by a factor of 5. The results are shown in Figure 15. The Curie temperature T_c has increased by 9 Kelvin as a result of the stronger magnetic field. This makes sense, as the stronger magnetic field will make it more favorable for the spins to point in the positive z-direction, thus requiring a higher temperature to randomize the orientations of the spins. The magnetization did not seem to reach zero, even at higher temperatures than shown in the plot, and seemed to stabilize at around 0.07, this could be due to the magnetic field contributing to a slightly higher amount of spins oriented in the positive z-direction.

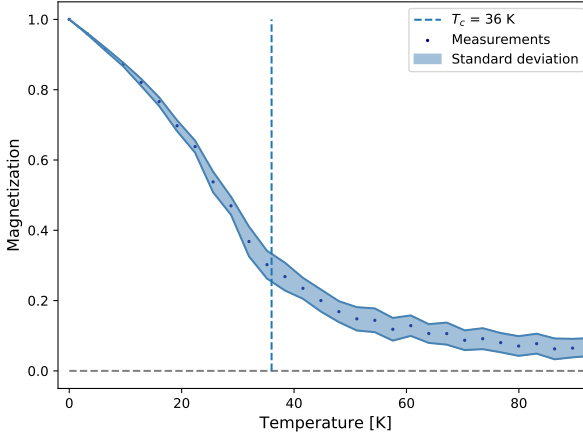


Figure 15: Plot of the temperature dependence of the magnetization at $\mu_s B_0 = 0.5J$. The Curie temperature T_c was estimated to be 36 Kelvin.

One last plot was made with the magnetic field reduced by a factor of five. The results are shown in Figure 16. The Curie temperature was taken as 22 Kelvin, the uncertainties was quite large around this point, however. The standard deviation seems to be the largest at the points in the vicinity of the Curie temperature. This could be due to the graph being at its steepest point at this temperature, meaning that the magnetization fluctuates more around this point. It is also possible that the system takes longer time to reach equilibrium in lower magnetic fields, such that

the temporal average was taken too soon. By increasing the time steps before taking the temporal average, the standard deviations of this plot could be lowered.

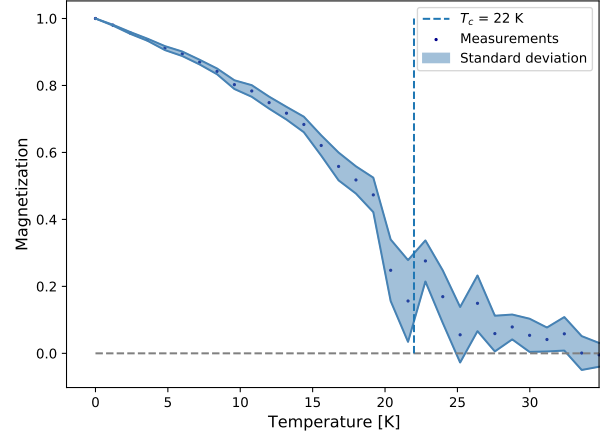


Figure 16: Plot of the temperature dependence of the magnetization at $\mu_s B_0 = 0.02J$. The Curie temperature T_c was estimated to be 22 Kelvin.

It is clear from the three graphs that the Curie temperature increases with an increased magnetic field. As mentioned above, this makes sense, as a stronger magnetic field makes it more favourable for the spins to be oriented in the positive z-direction, thus demanding a higher temperature to reach the paramagnetic phase.

Excercise 2

Ludvig Lous

April 2022

1 Task 1

I didn't quite have the time to write the derivation of the reduced Euler scheme into the report. The main process was to substitute the relations in (2.10) in the lab text into the regular Euler scheme, then I got the reduced Euler scheme as shown in (2.9).

2 Task 2

The Euler scheme can be used in this simulation as the force is linear in all regions of the ratchet. Thus, with a small enough time step, the force times the time step results in a good approximation.

3 Task 3

The functions was implemented in reduced units. By expressing equation 2.5 found in the exercise text in reduced units, I found that if $0 \leq \hat{x} < \alpha$, the potential would be $\frac{x}{\alpha} \Delta U$, and the force would be $\frac{1}{\alpha}$. Similarly, if $\alpha \leq \hat{x} < 1$, the potential would be $\frac{1-\hat{x}}{1-\alpha} \Delta U$, and the force would be $\frac{-1}{1-\alpha}$. When expressing $f(t)$ in reduced units, I got that $f(t) = 0$ for $0 \leq \hat{t} < \frac{3\tau\omega}{4}$, and $f(t) = 1$ for $\frac{3\tau\omega}{4} \leq \hat{t} < \tau$.

The functions which returned the potential and the force as a function of position and time was implemented by taking the modulus of t with respect to $\tau\omega$. I then divided the resulting number by $\tau\omega$, if the number i got was between 0 and 3/4, the functions would return 0, if it was between 3/4 and 1, the function would proceed to check the position. The x position was checked by taking the modulus of x

with respect to 1. If the resulting number was lower than α , which in this case was set as 0.2, the functions would return the potential and force described above for $0 \leq \hat{x} < \alpha$. If the resulting number was higher than α and less than 1 the functions would return the potential and forces for $\alpha \leq \hat{x} < 1$.

4 Task 4

The Gaussian distributed random numbers were generated using the Box-Muller algorithm. This algorithm consists of first generating two random numbers x_1 and x_2 from a uniform distribution between 0 and 1, and then plugging these numbers into the two equations $X = \sqrt{-2\ln(x_2)}\cos(2\pi x_1)$ and $Y = \sqrt{-2\ln(x_2)}\sin(2\pi x_1)$. X and Y will then be Gaussian distributed random numbers. Figure 1 shows the generations of Gaussian distributed numbers for different numbers of iteration. As seen in the figure, the numbers fit the Gaussian curve with mean 0 and standard deviation of 1 better for higher numbers of iterations.

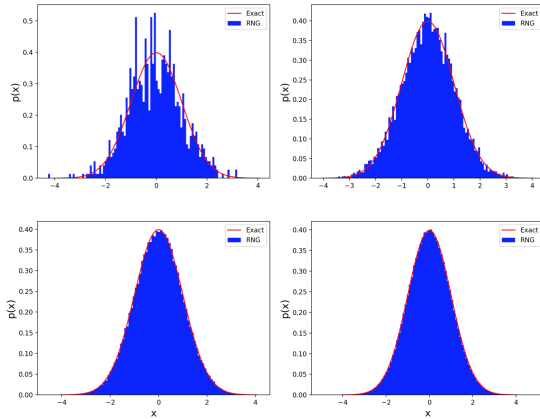


Figure 1: Normalized histograms of Gaussian distributed random numbers plotted against a Gaussian curve with a mean of 0 and a standard deviation of 1. The histograms were generated from 10^3 numbers (top left), 10^4 numbers (top right), 10^5 numbers (bottom left) and 10^6 numbers (bottom right).

5 Task 5

The reduced Euler scheme from equation 2.9 was implemented by taking in the position and time and calculating the resulting force acting on the particle using the reduced force function from Task 3.

6 Task 6

The criterion for the time step was converted to reduced units, which resulted in the equation

$$\max \left| \frac{\partial \hat{U}}{\partial \hat{x}} \right| \delta \hat{t} + 4 \sqrt{\frac{4k_B T \delta \hat{t}}{\Delta U}} << \alpha \quad (1)$$

To find a low enough time step, I created a while loop which ran until the left term of (1) was lower than 0.1α . The time step was multiplied with 0.8 between each iteration.

The constants were set to the values presented in Task 6 of the exercise text.

7 Task 7

With the flashing turned off, meaning that the potential is always turned on, the particle trajectory was simulated for $\Delta U = 0.1k_B T$. The results are shown in Figure 2. The particle is able to jump over the potential barrier for such a low ΔU , as seen in the plot.

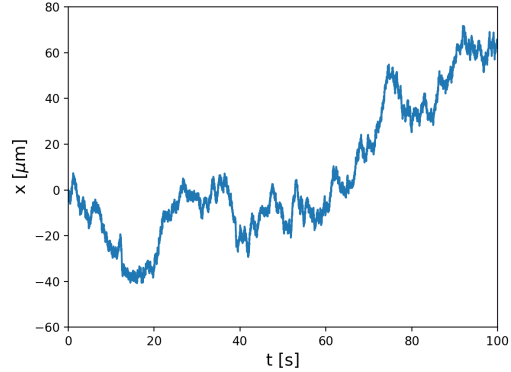


Figure 2: Simulation of the particle trajectory with $\Delta U = 0.1k_B T$

Another simulation of the particle trajectory was done, but this time with $\Delta U = 10k_B T$. The results can be seen in Figure 3. As seen in the figure, the higher potential barrier causes the particle to be stuck inside its starting well, as it doesn't have the energy to overcome the potential barrier of $10 k_B T$.

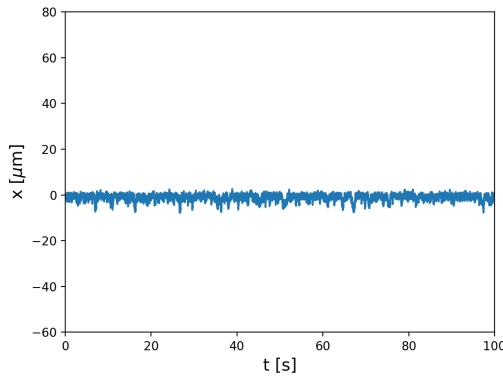


Figure 3: Simulation of the particle trajectory with $\Delta U = 10k_B T$

The distribution of occupied potential energy for these simulations was compared with the Boltzmann distribution given in (2.11) in the exercise text. This was done by taking the time and position of the particle for each step in the trajectory, and using the reduced potential function from Task 3 to return their potential energy. The energies were plotted as a normalized histogram and compared to the Boltzmann distribution. The occupied energies for $0.1 k_B T$ are shown in Figure 4. The occupied energies fits relatively well with the Boltzmann distribution.

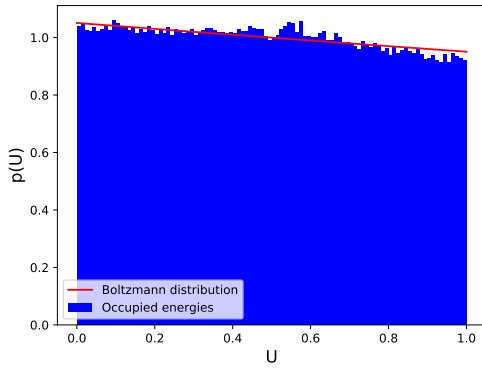


Figure 4: Occupied energies compared with the Boltzmann distribution at $\Delta U = 0.1k_B T$

A comparison of the occupied energies compared to the Boltzmann distribution at $\Delta U = 10k_B T$ is shown in Figure 5. Although both plots contains the same amount of data points, the distribution fits even better here. This is probably due to the particles having less freedom to move with a higher potential barrier, compared to the lower potential where the particle can travel over much greater distances. This increases the randomness of the position, allowing for greater variation in energies.

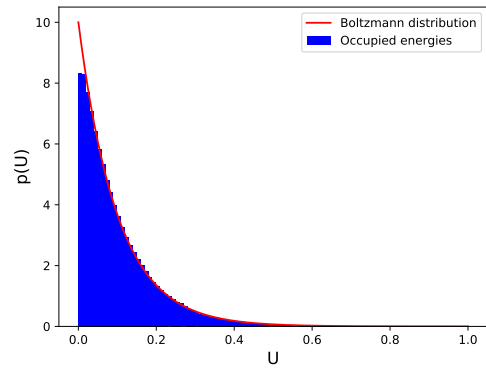


Figure 5: Occupied energies compared with the Boltzmann distribution at $\Delta U = 10k_B T$

8 Task 8

The potential barrier ΔU should be set fairly high, such that the particle is trapped in its current potential well. When the potential is later turned on, the particle is free to move. The key to ensuring net drift to the right is to set α to a value like 0.2 such that the potential is steeper at the right end. If you find a suitable flashing period, you can make it probable that the particle can diffuse across this steeper region to the well to the right, while it is still improbable that the particle can diffuse to the well to the left, as this would require a longer distance to diffuse, and thus requiring a longer amount of time on average.

If the flashing period τ is too short, the particle will not have time to diffuse to the well to the right either, causing it to be stuck in its current well. If

the flashing period is too long however, the particle will be able to drift to the neighbouring well with a significant probability. This will cause the particle to be able to jump in both directions. An optimal flashing period would thus be something in between, where there is only a significant probability that the particle will jump to the right when the potential is turned off.

9 Task 9

The particle trajectory was first simulated with a period τ of 0.05 s. The results are shown in Figure 6. As seen in the figure, the particle does not move from its initial well. Due to the low value of τ , the particle does not have enough time to diffuse to the well to the right before the potential is turned on again, at is it pushed back to the well.

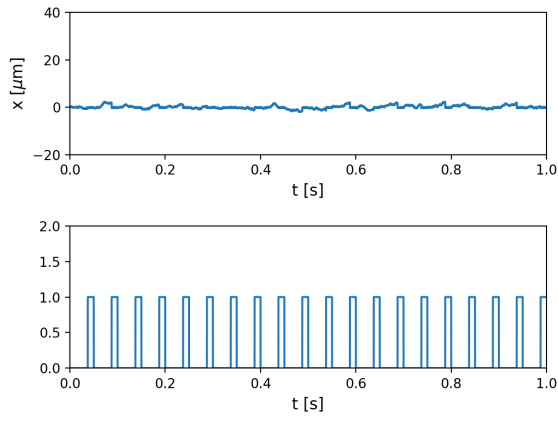


Figure 6: Upper: Trajectory of the particle at $\tau = 0.05s$, Lower: The plot shows when the potential is turned on and off (a value of 1 when the potential is turned on).

Next, the particle trajectory was simulated with a period of $\tau = 1s$. The trajectory of the particle is shown in Figure 7. Here, the particle is shown to jump to the right (right being the positive x-value) when the potential is turned off. It does not seem to have enough time to jump to the left, however.

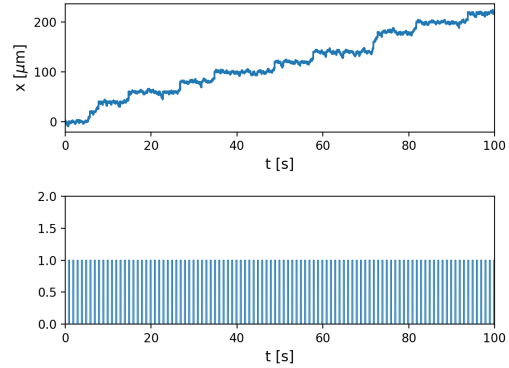


Figure 7: Upper: Trajectory of the particle at $\tau = 1s$, Lower: The plot shows when the potential is turned on and off (a value of 1 when the potential is turned on).

Finally, the particle trajectory was simulated with $\tau = 50s$. The results are shown in Figure 8. The particle is seen to have a net movement to the right, it does however also jump to the left at some stages. This is due to the high value of τ , which gives the particle a probability to move in the left direction as well.

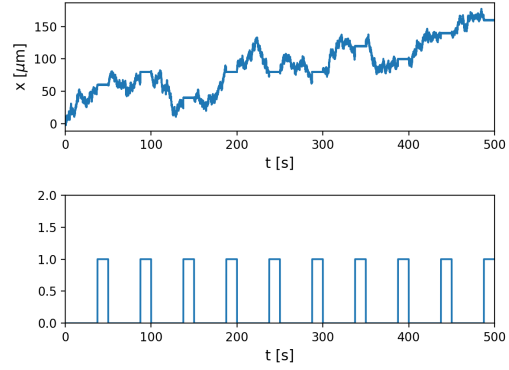


Figure 8: Upper: Trajectory of the particle at $\tau = 50s$, Lower: The plot shows when the potential is turned on and off (a value of 1 when the potential is turned on).

The average drift velocity $\langle v \rangle$ was computed for 80 flashing periods ranging between 0.1 and 2τ by taking the end position of the particle and dividing it by the time passed. For each τ , the average of 50 simulations was used. The results can be seen in Figure 9. The optimal flashing period τ_{opt} was found to be 0.48 s through using the numpy function polyfit which fitted a fifth-degree polynomial to the measured drift velocities, and taking the maxima of this polynomial in this interval. The drift velocity at τ_{opt} was found to be $5.48 \mu\text{m/s}$. The standard deviations are quite high as seen in the figure. This indicates that there is a high uncertainty in how far the particle will travel in a given amount of time.

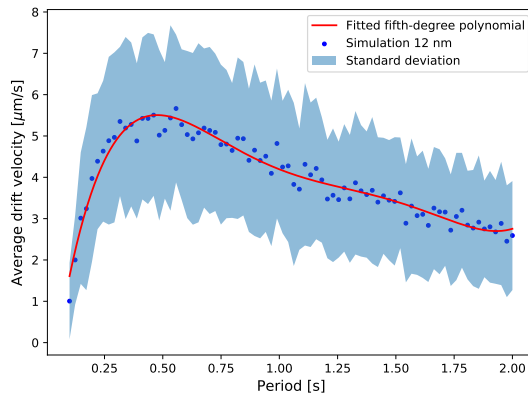


Figure 9: Drift velocity of a 12 nm particle $\langle v \rangle$ as a function of the flashing period τ .

10 Task 10

In the experiment, the flashing had a frequency of 0.7 Hz, which corresponds to a flashing period τ of 1.43 s. From Figure 9, the average drift velocity at this flashing period was found to be $3.51 \mu\text{m/s}$. As the length between each well in the experiment was 20 μm , one can read from Figure 10 that the particles had travelled somewhere between 40 and 60 μm on average after 10 cycles. From our flashing period τ , we get that this translates to 14.3 s. By multiplying the average drift velocity by the time passed, we get 48.1 μm . This corresponds fairly well with the results

from Figure 10.

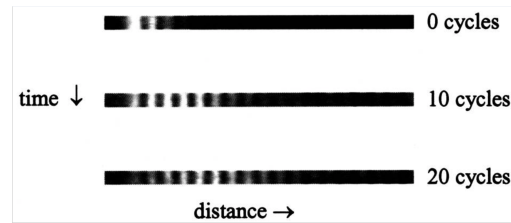


Figure 10: Trajectory of particles from the attached experiment report.

11 Task 11

The friction constant of the particle is given by $\gamma_i = 6\pi\eta r_i$, and the constant ω is related to γ_i through the relation $\omega = \frac{\Delta U}{\gamma_i L^2}$. As the reduced time unit is related to the ordinary time through the relation $\hat{t} = \omega t$, one can see how the reduced time \hat{t} will become lower in relation to the ordinary time with an increased r_i .

As the relation between \hat{t} and the ordinary time is decreased by a factor of three with a tripling of the radius, I would expect the drift velocity of a particle with radius $r_2 = 3r_1$ to be approximately

The plot of the drift velocities for a particle with radius $r_2 = 36 \text{ nm}$ plotted over periods between 0.1 to 3 s is shown in Figure 11. The optimal period was found to be 1.37 s, here the drift velocity was found to be $1.81 \mu\text{m/s}$. The drift velocity of the particle at τ_{opt} for the 12 nm particle was found to be $1.04 \mu\text{m/s}$.

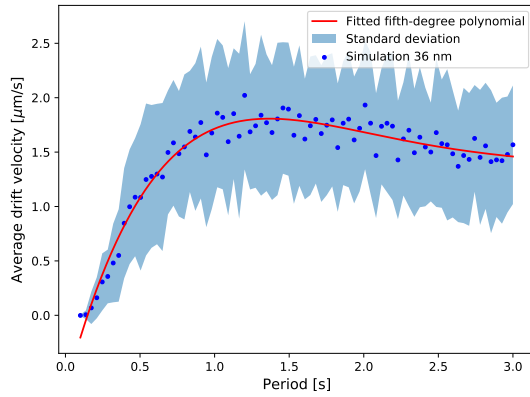


Figure 11: Drift velocity of a 36 nm particle $\langle v \rangle$ as a function of the flashing period τ .

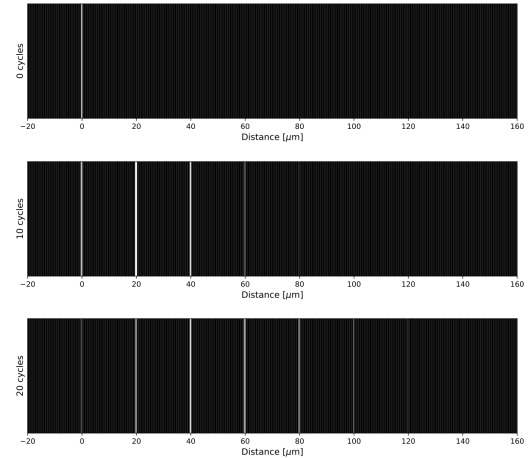


Figure 12: Diffusion of 1000 particles with a radius of 12 nm after 0, 10 and 20 cycles.

The same simulation was done with particles of 36 nm, the results are shown in Figure 13. The expected average drift length after ten cycles is $24.8 \mu\text{m}$, and $49.6 \mu\text{m}$ after 20 cycles. This seems to correspond somewhat well with the results from Figure 13, but again, the estimated drift velocities are quite uncertain.

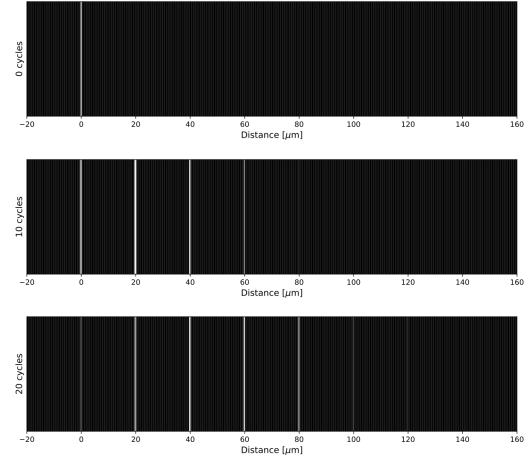


Figure 13: Diffusion of 1000 particles with radius of 36 nm after 0, 10 and 20 cycles.

12 Task 13

1000 particles with radius 12 nm was simulated over 0, 10, and 20 cycles. The results are shown in Figure 12. As seen in the figure, the particles gradually move towards the right. The expected average drift length is $26.3 \mu\text{m}$ after ten cycles, and $52.6 \mu\text{m}$ after 20 cycles. This seems to be a bit higher than the results in Figure 12. This could be due to the high standard deviation in Figure 9, making the predicted drifts quite uncertain.